Volume 25
Number 15
7 August 2025
Pages 3583–3870

Lab on a Chip

Devices and applications at the micro- and nanoscale

rsc.li/loc

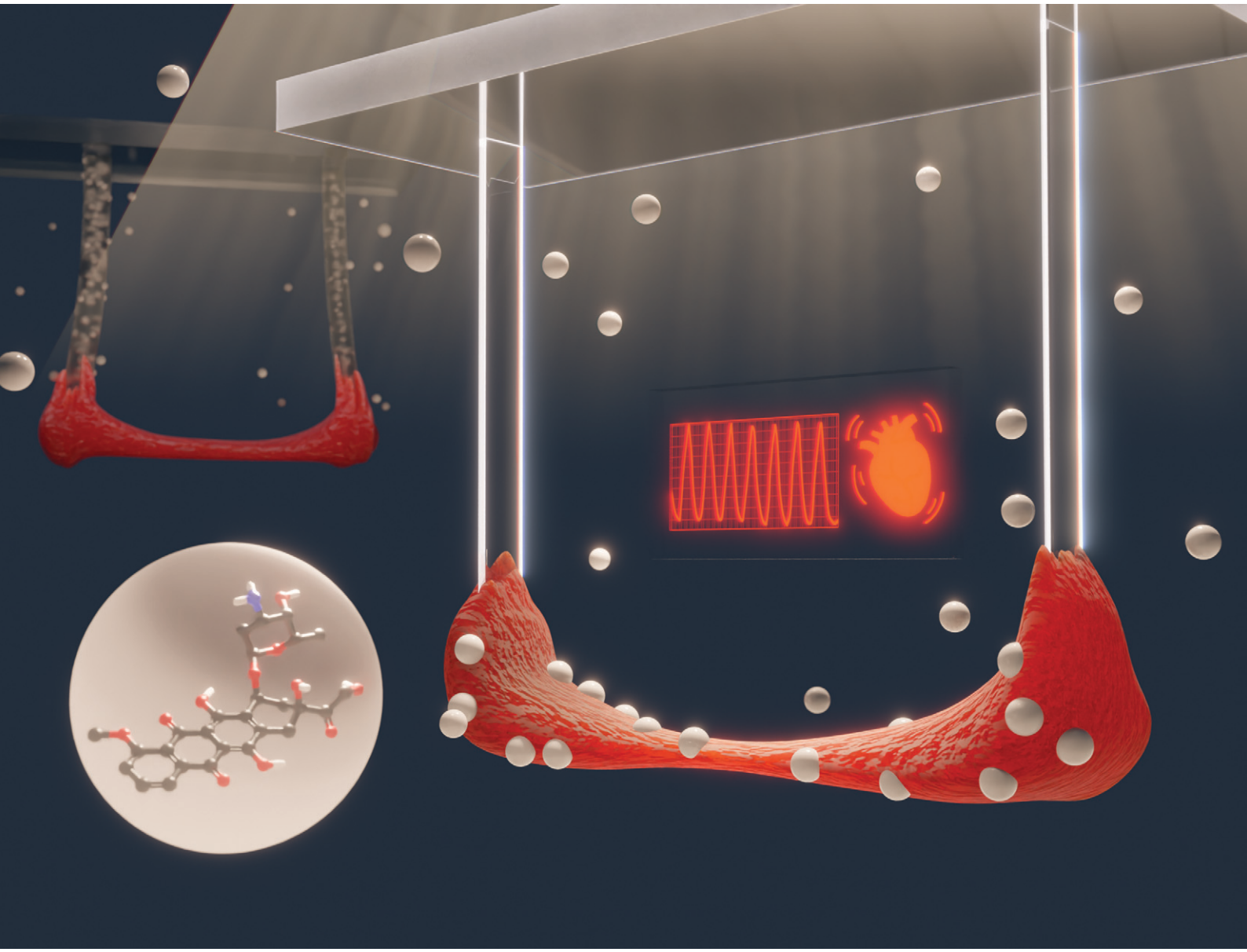

ISSN 1473-0197

ROYAL SOCIETY OF CHEMISTRY

PAPER

Yuya Fujiwara, Yoshinori Yoshida *et al.*
A polystyrene-film-based device for engineered cardiac tissues enables accurate analysis of drug responses on contractile properties

Lab on a Chip

PAPER

View Article Online
View Journal | View Issue

Cite this: *Lab Chip*, 2025, **25**, 3682

A polystyrene-film-based device for engineered cardiac tissues enables accurate analysis of drug responses on contractile properties†

Yuya Fujiwara,*[ab] Masako Sasaki,[ab] Sohei Funaoka,[c] Takuro Yoshikuni,[c] Yuki Naka,[ab] Kazumi Ida,[ab] Taichi Aihara,[c] Shunsuke Funakoshi,[ab] Kenichi Imahashi[bd] and Yoshinori Yoshida *[ab]

Engineered heart tissues (EHTs) using human induced pluripotent stem cells provide a valuable *in vitro* platform for assessing pharmacological and toxicological effects on cardiac functions. EHT devices offer a feasible approach to readily evaluate drug responses on contractile properties, including contractile force and relaxation, by measuring the moving distance of pillars attached to EHTs. However, the absorption of small molecule compounds by polydimethylsiloxane (PDMS), the material commonly used to construct EHT devices, hinders the accurate evaluation of the pharmacodynamic properties of drug candidates on contractility. Here, we developed a low-absorption EHT device using polystyrene (PS) to address this issue. Moreover, we generated an original Python-based analysis program to avoid analytical bias when tracking pillar positions and analyzing the contractile waveform drawn from EHT movements. This analytical platform enables the detection of increased contractile force during EHT maturation and the negative inotropic effects of diltiazem and blebbistatin on EHT contractile functions. Moreover, EHTs with PS-based devices suppressed the absorption of a cardiotoxic drug, doxorubicin, thus allowing the detection of cardiotoxic effects even at low concentrations compared to EHTs grown on PDMS-based devices. Together, our EHT system represents a useful *in vitro* platform for accurate evaluations of drug responses by the human heart.

Received 20th August 2024,
Accepted 2nd April 2025

DOI: 10.1039/d4lc00691g

rsc.li/loc

Introduction

During drug development, the efficacy and toxicity of newly developed drugs are primarily tested using animal models, including rodents and nonhuman primates, followed by human clinical trials. However, 76% of drugs failed in phase II and phase III clinical trials due to a lack of efficacy and safety between 2013 and 2015.[1] Interspecies differences between humans and experimental animals are often viewed as a significant contributing factor to such shortcomings.[2]

As an alternative to animal models, *in vitro* 3D heart tissue models using human induced pluripotent stem cell derived-cardiomyocytes (hiPSC-CMs) represent a novel yet accurate approach for *in vitro* drug testing and disease modeling that faithfully recapitulates human heart pathophysiology.[3–6] These platforms have been constructed as various structures, including strips,[7–10] sheets,[11–13] rings,[9,14] and chamber-like structures,[15] and offer valuable pharmacodynamics insights for potential drug candidates. Among these platforms, engineered heart tissues (EHTs) with a strip-like structure anchored on both sides by elastic pillars are most commonly employed because they enable quantitative evaluations of contractile functions from pillar displacement based on beam theory without specialized equipment.[10,16–20]

Polydimethylsiloxane (PDMS), known for its high biocompatibility and flexible characteristics, has been utilized as a material for EHT devices.[7,10] However, a significant drawback of PDMS is its characteristically high absorption of small molecule compounds, which impedes the accurate evaluation of their pharmacological and toxicological effects.[21–23]

To overcome this issue in PDMS-based devices, we developed a low-absorption EHT device using polystyrene (PS) and an analysis program for bias-free evaluations of contractile functions by measuring pillar displacement. This

[a] *Center for iPS Cells Research and Application, Kyoto University, Japan. E-mail: yuya.fujiwara@cira.kyoto-u.ac.jp, yoshinor@cira.kyoto-u.ac.jp*
[b] *Takeda-CiRA Joint Program, Fujisawa, Japan*
[c] *Sumitomo Bakelite Company Limited, Kobe, Japan*
[d] *Global Advanced Platform, Takeda Pharmaceutical Company Limited, Fujisawa, Japan*

† Electronic supplementary information (ESI) available: The numerical data in each graph. See DOI: https://doi.org/10.1039/d4lc00691g

platform prevents the undesired absorption of drugs into devices, enabling the examination of drug effects even at low concentrations, thus leading to accurate and automatic evaluation of these effects on human heart tissues.

Materials and methods

Device construction

PS films were produced by punching PS sheets into the prescribed shape. Other device components such as plastic supports, caps used to fix pillars to plastic supports, and casting mold containers were also made of PS. EHT devices were assembled using these components. Weights were attached to the tip of pillars to measure the moving distance of PS film pillars associated with loads of 2.9, 7.1, 11.6, and 24.4 mg, with the displacement of pillar tips from the initial position measured by digital microscopy. PDMS-based devices used were commercially available (EHT Technologies).

Cell culture and differentiation

The hiPSC line, 1390D4 (CiRA), was cultured in StemFit®AK02N (Ajinomoto) on iMatrix-511 (Nippi)-coated dishes. Human cardiac fibroblasts (HCFs) (Promo Cell) were cultured in a Fibroblast Growth Medium 3 kit (Promo Cell). The cardiomyocyte differentiation method using embryoid bodies (EBs) was previously described.[3] For cardiomyocyte purification, day 10–15 EBs were cultured in DMEM without glucose, L-glutamine, and phenol red (Thermo Fisher) supplemented with 4 mM L-lactic acid (Wako) and 1 mM sodium pyruvate (Thermo Fisher Science) for 3 days. The EBs were subsequently cultured in a culture medium composed of StemPro-34 SFM (Thermo Fisher Science) supplemented with 2 mM L-glutamine (Invitrogen), 0.4 mM monothioglycerol (Sigma), 50 μg mL^{-1} ascorbic acid (Sigma), 150 μg mL^{-1} transferrin (Wako), and 5 ng mL^{-1} VEGF. All experiments involving human iPS cells were conducted in accordance with regulations set forth by the ethics committees of Kyoto University Graduate School and Faculty of Medicine.

Engineered heart tissue (EHT) generation

For preparing dissociated EBs into single cardiomyocytes, day 2–7 EBs cultured after purification were incubated with 10–20 μg mL^{-1} Liberase™ (Sigma-Aldrich) in IMDM (Thermo Fisher Scientific) for more than 1 h, which was changed to TrypLE Select (Thermo Fisher Scientific) supplemented with 10 μg mL^{-1} DNase I for 10 min at 37 °C. After adding an equal volume of culture medium, EBs were dissociated by pipetting. Dissociated hiPSC-CMs were mixed with HCFs at a 9 : 1 ratio in 100–150 μL culture medium supplemented with 10 μM Y-27632, 2.5–5 mg mL^{-1} fibrinogen (Sigma-Aldrich), 10% fetal bovine serum, 5–20 μg mL^{-1} aprotinin, 0.75–3 units thrombin, and 10% Geltrex™ LDEV-free reduced growth factor basement membrane matrix (Invitrogen Corporation). For evaluating maturation and drug effects, EHTs were mixed with 6.75×10^5 hiPSC-CMs and 0.75×10^5 HCFs in a 9 : 1 ratio. For comparison between PS film- and PDMS-based devices, EHTs were mixed with 8×10^5 hiPSC-CMs and 2×10^5 HCFs at an 8 : 2 ratio. Cell mixtures were seeded into troughs of device-attached molds and incubated for over 1 h. After incubation, 1000 μL IMDM was added, and EHT-attached devices were transferred into new wells and cultured in the culture medium supplemented with or without 10 μM Y-27632. The culture medium was changed once every 3–5 days. For EHT maturation, day 7 EHTs were cultured in DMEM containing 2 mg mL^{-1} glucose (Thermo Fisher Scientific) supplemented with 1/100 B27 minus insulin (Thermo Fisher Scientific), 5–20 μM palmitate (Sigma-Aldrich), 0.25 μM dexamethasone (Dex) (Sigma-Aldrich), 6 nM 3,3′,5- triiodo-L-thyronine (T3) (Sigma-Aldrich), 1 μM GW7647 (Merck), 50 μg mL^{-1} ascorbic acid (Sigma-Aldrich), 100 U mL^{-1} penicillin, and 100 μg mL^{-1} streptomycin (Thermo Fisher Scientific) for 9 days. After 9 days of treatment, EHTs were maintained in DMEM containing 2 mg mL^{-1} glucose supplemented with B27 minus insulin, 5–20 μM palmitate, 50 μg mL^{-1} ascorbic acid, 100 U mL^{-1} penicillin, and 100 μg mL^{-1} streptomycin. Immature EHTs were cultured in DMEM containing 4.5 mg mL^{-1} glucose (Thermo Fisher Scientific) supplemented with B27 minus insulin, 50 μg mL^{-1} ascorbic acid, 100 U mL^{-1} penicillin, and 100 μg mL^{-1} streptomycin after day 7.

Image-based contraction measurement

After 2–5 days of maturation, EHTs were washed with PBS and incubated in pre-warmed modified Tyrode's solution (129 mM NaCl, 1 mM $MgCl_2$, 2.5 mM KCl, 2 mM $CaCl_2$, 30 mM D-glucose, and 25 mM HEPES pH 7.5) for 30 min at 37 °C with 5% CO_2. For measuring EHT contractile functions, videos of EHTs contracting were recorded using a fluorescence microscope (BZ-X880, KEYENCE) for 5 s under 1.5 Hz electrical pacing.

To measure acute drug responses by blebbistatin (Sigma-Aldrich) and diltiazem (FUJIFILM Wako Pure Chemical Corporation), after incubation in pre-warmed modified Tyrode's solution for 30 min, EHTs were incubated in pre-warmed modified Tyrode's solution containing 1/1000 volume of vehicle (DMSO) at 37 °C with 5% CO_2 for 15–30 min. Subsequently, 5 second videos were recorded under 1.5 Hz electrical stimulation as the baseline. Next, EHTs were incubated in pre-warmed modified Tyrode's solution containing 1/1000 volume of the lowest concentration of each compound at 37 °C with 5% CO_2 for 15–30 min, followed by 5 second video recordings under 1.5 Hz electrical stimulation. This procedure was repeated for all increasing concentrations tested in this study.

To measure doxorubicin (MedChemExpress)-mediated cardiotoxicity, EHTs cultured for 1–5 days after maturation were incubated in pre-warmed modified Tyrode's solution at 37 °C with 5% CO_2 for 30 min, and 5 second videos of pre-

treatment EHT contractions were recorded. Subsequently, recorded EHTs were cultured in DMEM containing 2 mg mL^{-1} glucose and supplemented with B27 minus insulin, 5–20 μM palmitate, 50 μg mL^{-1} ascorbic acid, 100 U mL^{-1} penicillin, and 100 μg mL^{-1} streptomycin containing the indicated doxorubicin concentrations for 3 days. Following doxorubicin treatment, EHTs were incubated in pre-warmed modified Tyrode's solution at 37 °C with 5% CO_2 for 30 min, and 5 second videos of post-treatment EHT contractions were recorded.

Contraction analysis using a Python-based program

The contraction analysis program was built in the Python environment, and the main libraries used were as follows: OpenCV was used for video input/output and pillar tracking, and multiple instance learning (MIL) was used as the tracking algorithm. Numpy and Pandas were used for numerical computations. Matplotlib was used for graph drawing. SciPy was used for waveform peak detection.

Parameters, including the scale and frequency of electrical stimulation, were set into the program, and a video was loaded using the OpenCV library. For tracking pillars, a pillar was manually selected as a region of interest (ROI) in the first frame of the video, and pillar displacement was automatically tracked in subsequent frames. For tracking accuracy confirmation, the tracking process was outputted as a video (mp4 format). For defining the contraction baseline, either the highest values of the ROI x-coordinates from the upper left vertex or the average of the highest and lowest values in the most frequent pillar position of the ROI x-coordinate (with the data divided into 40 classes) was defined as the baseline. The displacement of the ROI from the baseline over time was drawn and smoothed using a moving average ($n = 3$).

The highest value of each contraction waveform obtained was defined as the contraction peak. The lowest value before the peak point of each contraction was defined as the baseline of a contraction. The 20% contraction point in each contraction was estimated by linear interpolation using the nearest point before and after 20% displacement between the baseline and peak. The 80% relaxation point in each contraction was estimated by linear interpolation using the nearest point before and after 80% displacement between the peak and baseline of the next contraction. The pillar displacement in each contraction was defined as the value from the starting point to the peak. The contractile force of EHTs using PS film-based devices was calculated using the following equation:

$$\text{Contraction force } (N) = \frac{b \times h^3 \times E \times W}{4 \times l^3}$$

where b is the width (2 mm), h is the thickness (0.05 mm), E is the Young's modulus (2611 MPa), W is the displacement (mm), and l is the length (11.3 mm).

The contractile force of EHTs using PDMS-based devices was calculated using the following equation:

$$\text{Contraction force } (N) = \frac{3 \times \pi \times E \times d^4 \times W}{4 \times l^3}$$

where d is the radius (0.5 mm), E is the Young's modulus (1.7 MPa), W is the displacement (mm), and l is the length (12 mm).

The contraction and relaxation times were calculated as the time between the peak and 20% or 80% relaxation points, respectively. The average of three consecutive contraction waveforms was used as a data point for each EHT.

Since the contractile force of EHTs follows Hooke's law, contractile stress, the force normalized by the cross-sectional area of EHTs, was used to accurately compare the contractile force between different EHTs or across different days of culture for the same EHT. Pillar displacement was used to quantify the effects of drug treatments on the contractile force using the same EHTs on the same day.

Rhodamine B absorption measurement

PS and PDMS (CS CRIE) (1 cm × 1 cm × 50 μm) were incubated in IMDM (Thermo Fisher Scientific) containing 10 μM Rhodamine B for 24 hours. Following incubation, films were washed with PBS five times, and fluorescence and phase contrast images were captured using a fluorescence microscope (BZ-X880, KEYENCE). The fluorescence intensity was measured using ImageJ Fiji[24] to quantify Rhodamine B absorption.

Parallel transmittance measurement

Parallel transmittance of PS (50 mm × 50 mm × 50 μm) and PDMS (Asahi Rubber) (50 mm × 50 mm × 60 μm) was measured using a HAZE meter following the manufacturer's instructions.

Young's modulus measurement

Tensile strength tests were performed on PS (150 mm × 20 mm × 50 μm) and PDMS (Asahi Rubber) (150 mm × 20 mm × 60 μm) at tensile speeds of 5 mm min^{-1} and 500 mm min^{-1}, respectively. The Young's modulus was calculated from the results in the strength range of 10–20 N mm^{-2} for PS and 1–2 N mm^{-2} for PDMS.

Attachment rate of hiPSC-CMs onto PDMS and PS

Plasma-treated PS and PDMS (Asahi Rubber) (1 cm × 1 cm × 50 μm) were coated with either 0.1 mg mL^{-1} fibronectin or 5% Matrigel for over an hour in 24-well low-attachment culture plates (Corning). After coating, 2.5×10^5 purified hiPSC-CMs were cultured in a medium supplemented with 10 μM Y-27632 at 37 °C with 5% CO_2. The next day, after PBS washing, the attached hiPSC-CMs were fixed with 4% paraformaldehyde for 15 min at room temperature. The hiPSC-CMs were stained with an anti-cTNT antibody (Invitrogen), an Alexa647 anti-mouse IgG antibody (Invitrogen), and Hoechst33342 (DOJINDO). Fluorescence images were obtained using a fluorescence microscope (BZ-

X880, KEYENCE) with ×2 and ×10 objective lenses. To quantify the attached hiPSC-CMs, the cTNT-positive area in the images obtained using the ×2 objective lens was measured using ImageJ Fiji.[24]

Mitochondria staining

Purified hiPSC-CMs were seeded at 2.5×10^5 cells per well onto 0.1 mg mL^{-1} fibronectin-coated 24-well plates and cultured in a medium supplemented with 10 μM Y-27632 at 37 °C with 5% CO_2. After 1–2 days, for maturation, the hiPSC-CMs were cultured in the maturation medium for 9 days and then in the maturation medium without Dex/T3/GW7647 for 3 days. Immature hiPSC-CMs were cultured in the immature medium for 12 days at 1–2 days after seeding.

Calcium imaging

Prior to measuring calcium kinetics, maturation medium-treated EHTs were cultured in the maturation medium without Dex/T3/GW7647 for 2–4 days, and immature medium-treated EHTs were cultured in the immature medium for the same period. To measure the intracellular calcium content, EHTs were detached from devices and incubated in Gey's balanced salt solution (GBSS) containing 5 μM Calbryte520 (AAT Bioquest) and 0.04% Pluronic F-127 (Thermo Fisher Scientific) for 30–60 min at 37 °C with 5% CO_2. After removing the dye, EHTs were incubated in GBSS containing 10 μM blebbistatin (Sigma-Aldrich) for 15 min at 37 °C with 5% CO_2. Calcium imaging of EHTs was performed using an inverted fluorescence microscope (Nikon) under 1.5 Hz electrical pacing for 10 s. Images and signal intensity data at each time point were obtained using NIS-elements AR (Nikon). The data were analyzed using MATLAB software (MathWorks).

RNA extraction and qPCR

Day 17–18 matured EHTs were lysed using QIAzol (QIAGEN), and a miRNeasy Mini Kit (QIAGEN) was used for RNA purification following the manufacturer's instructions. Reverse transcription PCR was performed using a PrimeScript™ RT reagent kit (TAKARA). Quantitative PCR (qPCR) was performed using Taqman™ Fast Advanced Master Mix (Applied Biosystems) and TaqMan probes (TBP: Hs00427620_m1, TNNI1: Hs00913333_m1, TNNI3: Hs00165957_m1, ACTN2: Hs00153809_m1, MYH6: Hs01101425_m1, MYH7: Hs01110632_m1, CACNA1C: Hs00167681_m1, RyR2: Hs00181461_m1, ATP2A2 (SERCA2): Hs00544877_m1, KCNJ2: Hs01876357_s1, HCN4: Hs00975492_m1, SCN5a: Hs00165693_m1, GJA1: Hs00748445_s1, MT-ND1: Hs02596873_s1, MT-ND4: Hs02596876_g1). qPCR data were obtained and analyzed using a QuantStudio7 Flex (Thermo Fisher Scientific).

Medium composition analysis

EHTs treated with the maturation medium for 6 days were transferred to a fresh medium. After 3 days of culture, the supernatant was collected and analyzed using a BioProfile FLEX2 (Nova Biomedical).

Statistical analysis

For comparisons between two groups, statistical significance was determined using the paired or unpaired two-tailed *t*-test. For multiple comparisons, statistical significance between groups was analyzed using a one-way or two-way analysis of variance (ANOVA) followed by Tukey's honest significant difference test or Šídák's multiple comparison test using GraphPad Prism 9. All data were obtained from at least 3 independent experiments.

Results

Development of a low-absorption device using polystyrene films

As materials to prevent the absorption of small molecules, thermoplastics such as PS are one of the most attractive materials and are particularly appealing due to the variety of processing methods available to facilitate easy prototype fabrication.[25] Since Rhodamine B, a fluorescent dye, was used as a surrogate marker to quantify drug absorption due to its ease of measurement,[26] we compared the absorption capacity of Rhodamine B between PDMS and PS substrates of the same volume (1 cm × 1 cm × 50 μm) to evaluate the low-absorption properties of PS (Fig. 1A and B). DMSO (vehicle) was used as a negative control (−). While the absorption of Rhodamine B by PS was minimal, it was significantly higher in PDMS (Fig. 1B), demonstrating the advantage of using PS as a low-absorption material for EHT devices. Next, to assess whether PS is a suitable material for EHT devices, we compared its properties with PDMS, including elasticity, transparency, and biocompatibility. Although PS exhibited slightly lower transparency than PDMS, both materials transmitted more than 85% of light (Fig. 1C). In terms of elasticity, PS (2611 MPa) had a significantly higher Young's modulus than PDMS (4.8 MPa) (Fig. 1D). Regarding biocompatibility with hiPSC-CMs, their ability to attach to PS and PDMS was comparable when the materials were coated with fibronectin or Matrigel (Fig. 1E and F).

These results indicate that compared to PDMS, PS exhibits lower absorption, high transparency – though slightly lower than PDMS – and no toxic effects on hiPSC-CMs (Table 1). Therefore, besides its lower elasticity, PS represents a suitable material for fabricating low-absorption EHT devices.

To address the elasticity limitation, we developed thin PS film-based pillars (50 μm thickness) to allow sufficient bending under contractile force. In addition, we developed a casting mold coated by low attachment modification to prevent cell adhesion when fabricating strip-like tissues (Fig. 2A). Using this device, we tested whether these pillars adequately bent under load. Consistent with the formula based on beam theory, the displacement at the tips of pillars exhibited a linear relationship with the applied force, closely aligning with theoretical values (Fig. 2B), indicating

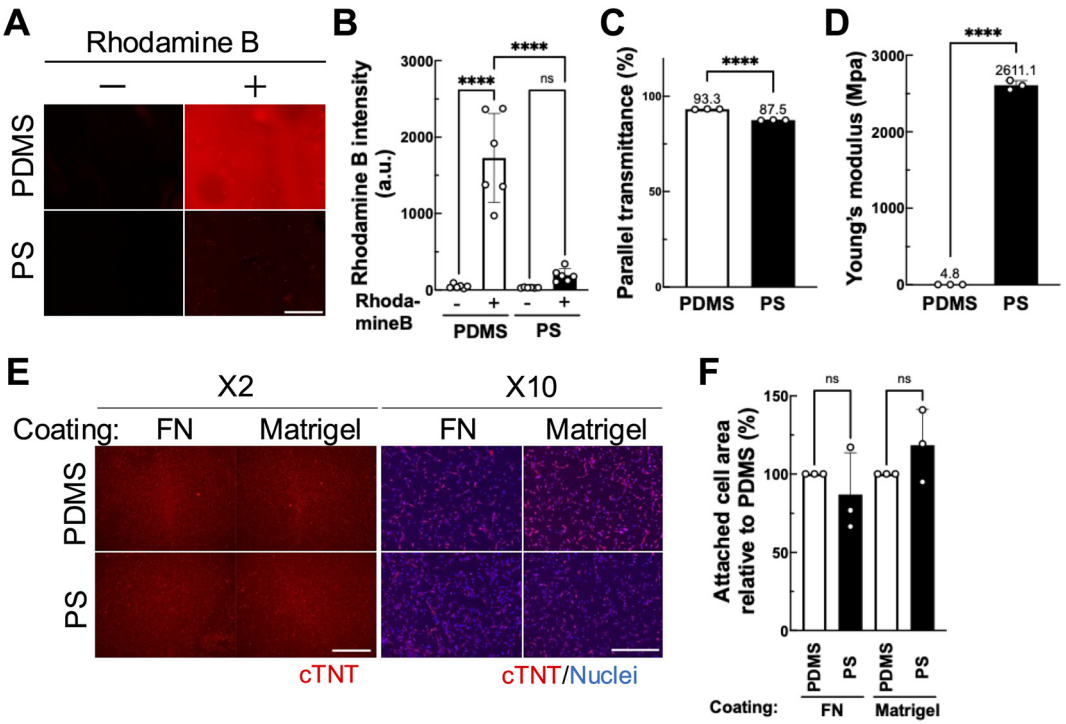

Fig. 1 Characteristics of PS as a material for EHT devices. (A) Fluorescence images of vehicle- (–) or Rhodamine B- (+) treated PDMS or PS. (B) Quantification of Rhodamine B intensity of vehicle- (–) or rhodamine B- (+) treated PDMS or PS from 3 independent experiments (n = 6). (C) Quantification of parallel transmittance of PDMS or PS from 3 independent experiments (n = 3). (D) Quantification of Young's modulus of PDMS or PS from 3 independent experiments (n = 3). (E) Representative immunostaining images of hiPSC-CMs attached to fibronectin- or Matrigel-coated PDMS or PS, obtained using 2× and 10× objective lenses for cTNT (red) and DNA (blue). Scale bar: 2000 μm (left panel), 500 μm (right panel). (F) Quantification of hiPSC-CM areas attached on the PDMS or PS substrate from 3 independent experiments (n = 3). Data are presented as the mean ± SD (B–D and F). Statistical analyses were performed using one-way ANOVA with Tukey's multiple comparison test (B and F) or unpaired t-test (C and D). **** indicates $p < 0.0001$. ns indicates not significant (B and F).

Table 1 Summary of comparison between PS and PDMS properties

Properties	Polydimethylsiloxane (PDMS)	Polystyrene (PS)
Absorption	High	Low (one-tenth of PDMS)
Transparency (parallel transmittance)	High (93.3%)	Slightly low (87.5%)
Elasticity (Young's modulus)	Low (4.8 MPa)	High (2611 MPa)
Biocompatibility	No difference for hiPSC-CMs	No difference for hiPSC-CMs

that the force applied to the tip of pillars can be accurately calculated based on distances between the relaxed and contracted pillar positions.

To generate EHTs, mixtures of hiPSC-CMs and primary HCFs were seeded onto a casting mold attached to the device. After incubating for an hour to allow the cell mixture to polymerize *via* the fibrinogen–thrombin reaction, tissues attached to pillars were transferred to new cell culture plates for further culture (Fig. 2C). EHTs gradually became compact during the next 7 days (Fig. 2D). Although EHTs with low cell density (2.5×10^5 cells per EHT) did not readily maintain tissue integrity, all EHTs with higher cell densities (7.5 and 10×10^5 cells per EHT) were successfully maintained for up to 14 days (Fig. 1D and E). Initially, straight pillars could not retain EHTs on day 0 (0/4), but the modified pillar structure significantly improved retention and success rates (4/4) (data not shown). This high success rate was attributed to the improved structural design of the pillar tips, allowing effective retention of EHTs.

Development of analysis programs to calculate contractile functions without bias

To accurately calculate the contractile properties of EHTs, we developed a program in the Python environment to measure pillar displacement. After manually setting the region of interest (ROI) based on the pillar position, the selected ROI was automatically traced, with the ROI displacement calculated. We analyzed the contraction waveforms using this program, which also outputted various data, including values of each parameter and a waveform graph (Fig. 3A). Since the left side of the video was defined as the x-axis origin, the program rotated the video by 180 degrees when analyzing a left-side pillar (Fig. 3B). Contractile forces were calculated

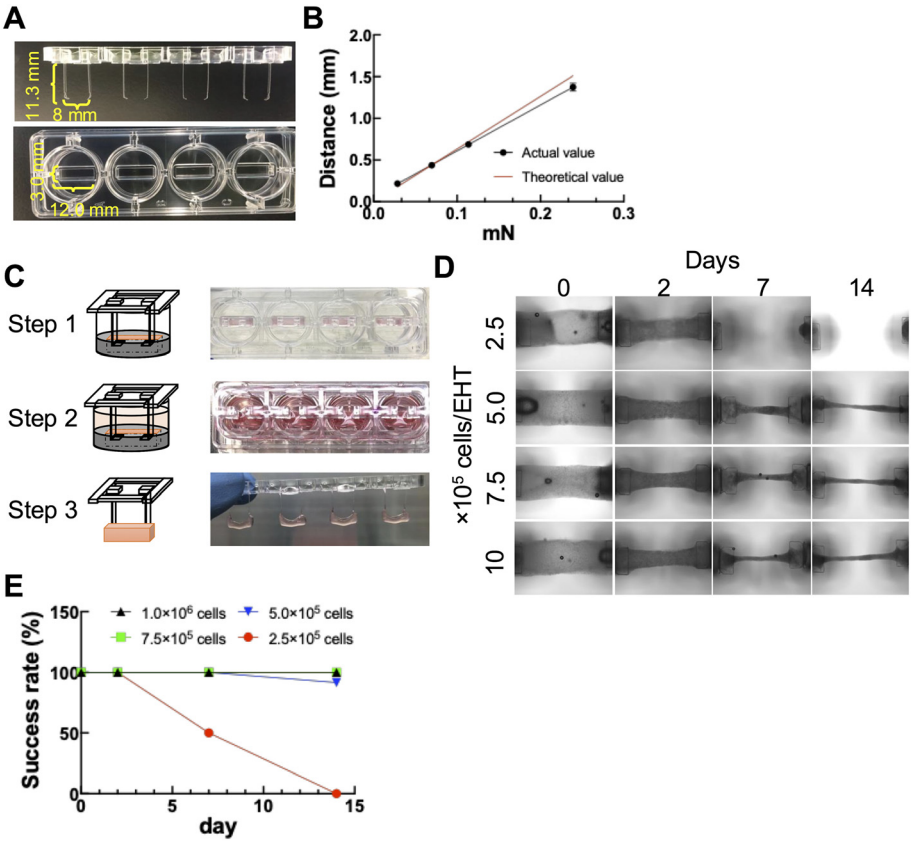

Fig. 2 Generation of PS film-based low-absorption devices. (A) Representative images of a PS film-based device (upper panel) and casting mold container (lower panel). (B) The relationship between pillar displacement and applied force (black line) (n = 8) and theoretical values (red line). (C) Illustration and representative images at each step during EHT construction. Step 1: cell mixtures were seeded into troughs of the casting mold container and incubated for 1 hour. Step 2: IMDM was added after incubation to remove EHTs easily from the casting mold container. Step 3: attached EHTs were removed from the device and transferred into new 24-well plates. (D) Representative images of EHTs at days 0, 2, 7, and 14 after EHT construction. (E) Success rates of EHT generation at days 0, 2, 7, and 14 after EHT construction from 4 independent experiments (n = 10–12).

from distances between peaks and troughs of the waveform. As illustrated in Fig. 3C, the contractile and relaxation times were defined as the time taken for the displacement to go from 20% of the amplitude to the peak during contraction and the time from the peak to the point where the displacement reaches 20% of the amplitude during relaxation, respectively (Fig. 3C). Values of contractile force, contractile time, and relaxation time were calculated as averages of the values from three consecutive waveforms.

hiPSC-CMs have been reported to exhibit immature phenotypes, including weak contractile force, low fatty acid utilization, high reliance on glucose as an energy source, and lack of T-tubules compared to mature adult cardiomyocytes.[27] To accurately manifest disease phenotypes and typical drug responses, as observed in the human heart, using EHTs derived from hiPSC-CMs, it is essential to promote EHT maturation.[3,28–30] Therefore, we applied our recently developed method incorporating multiple maturation factors, including hormones, PPARα agonists, and optimal energy substrates, to this EHT platform.[31] To evaluate whether our EHT platform can accurately detect the increment of contractile forces in EHTs treated with these maturation factors, we compared the displacement of pillars between mature EHTs and untreated immature EHTs (Fig. 4A). While the displacement was comparable between the right and left pillars under each condition, the displacement of mature EHTs was significantly increased compared to immature EHTs (Fig. 4B). Since the contractile force of EHTs follows Hooke's law, we evaluated the force normalized by the cross-sectional area of EHTs to compare the contractile force across different EHTs accurately. The result indicated that the contractile stress of mature EHTs was significantly higher than that of immature EHTs (Fig. 4C). Next, to confirm whether the increase in contractile stress was due to EHT maturation, we evaluated calcium handling and mitochondrial activity, both of which are known hallmarks of maturation. Mature EHTs exhibited increased calcium uptake kinetics compared to immature EHTs (Fig. 4D and E). Due to the difficulty of dissociating EHTs for mitochondrial activity assessment using fluorescent dyes, we measured mitochondrial activity in hiPSC-CMs instead. The results indicated that the mitochondrial activity was higher in mature hiPSC-CMs than in immature hiPSC-CMs, suggesting that a similar increase in mitochondria activity occurs in

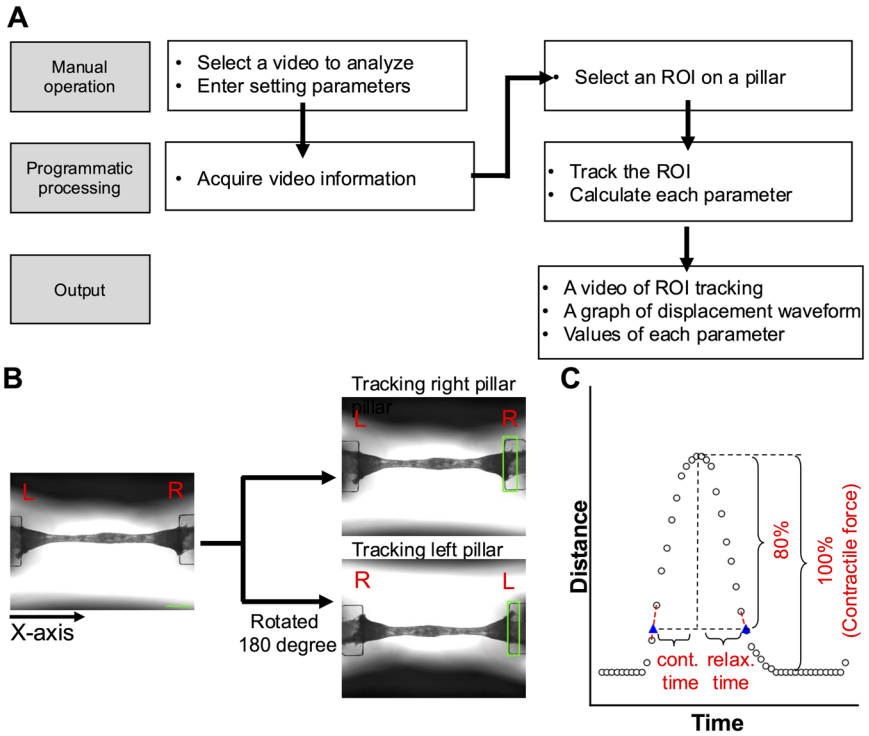

Fig. 3 Development of a contraction analysis program for engineered cardiac tissues. (A) Schematic flow diagram of the analytical process in the newly developed program. (B) Process flow of videos before pillar tracking. The left side in videos was defined as the *x*-axis origin. Green boxes indicate the region of interest (ROI) in the tracking region. L and R indicate the left and right sides in videos. Scale bar: 1000 μm. (C) Illustration of each contractile parameter. White circles indicate the measured value, and blue triangles indicate the 20% contraction and 80% relaxation points.

EHTs (Fig. 4D). Collectively, these results indicated that our EHT platform can accurately detect the changes in contractile stress between EHTs with different maturation states. We used these mature EHTs for all subsequent experiments.

Novel EHT platform detected concentration-dependent negative inotropic effects

To confirm whether our EHT platform can monitor acute changes in cardiac contractile properties in response to drug treatments, we applied several drugs with well-known effects on the human heart to our EHT platform. Blebbistatin, a myosin II inhibitor, reduced the contractile force of EHTs in a dose-dependent manner with an IC_{50} of 59 nM, along with significant decreases in both contraction and relaxation times (Fig. 5A and B). Since blebbistatin promotes myofilament uncoupling by reducing cross-bridge formation between actin and myosin,[32] this mechanism is likely responsible for reduced contraction and relaxation times.

Diltiazem, a calcium channel blocker, also decreased the contractile force in a dose-dependent manner with an IC_{50} of 317 nM, accompanied by significant decreases in both contraction and relaxation times (Fig. 5C and D). Diltiazem is known to shorten the action potential duration of hiPSC-CMs by blocking calcium ion influx,[33] which is consistent with our results (Fig. 5D). To further evaluate the utility of our EHT platform for monitoring cardiotoxic effects, we treated our EHTs with doxorubicin, a known cardiotoxic drug, for 3 days. While doxorubicin decreased the contractility of EHTs, with an IC_{50} of 300 nM (Fig. 5E), the contraction and relaxation times of EHTs remained unchanged even at a concentration of 300 nM doxorubicin (Fig. 5F). Although the detailed mechanisms affecting contraction and relaxation times in EHTs remain unclear, the doxorubicin-induced decrease in contractile force was not due to direct inhibition of the calcium channel or myosin, as observed with diltiazem and blebbistatin. Instead, it was primarily attributed to cytotoxic effects, resulting from factors such as mitochondrial dysfunction and DNA damage,[34] which are not expected to directly affect contraction or relaxation times.

Collectively, these results indicated that our EHT platform can accurately mimic drug responses observed in the human heart.

PS film-based devices accurately detected doxorubicin-induced cardiotoxicity due to their low-absorption feature

To evaluate the impact of drug absorption by EHT devices when evaluating drug responses, we compared doxorubicin-mediated effects between PDMS- and PS film-based EHTs (Fig. 6A). Given that EHT maturity affects drug responses,[29] we first compared mRNA expression levels of sarcomere-, sarcoplasmic reticulum (SR)-, and mitochondria-related

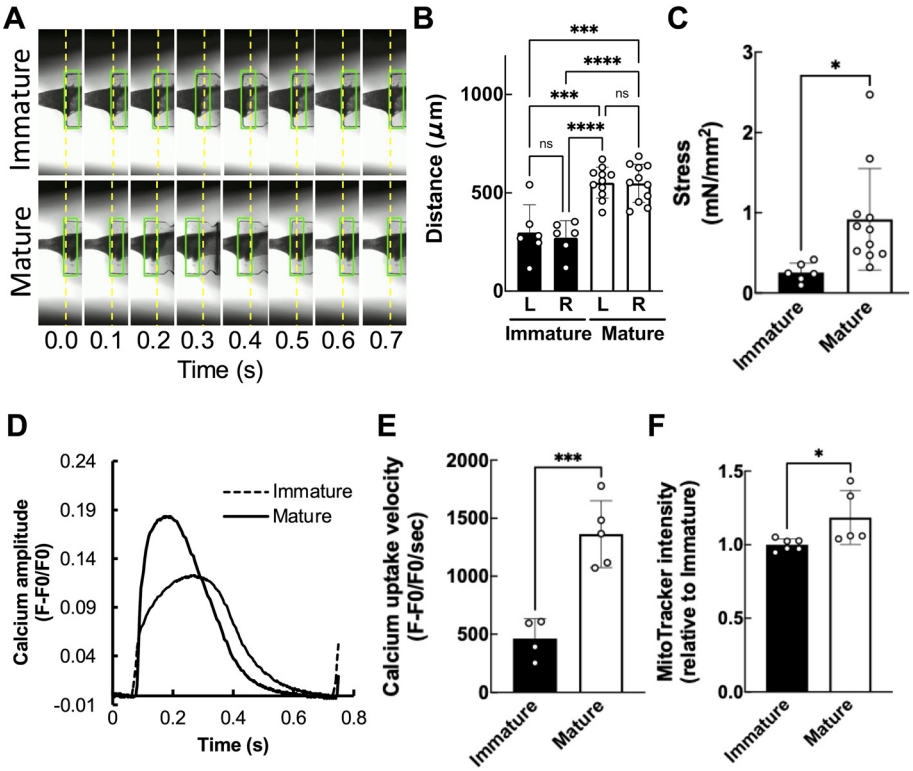

Fig. 4 Detection of contraction stress increments of EHTs. (A) Representative tracing results during one contraction period in day 17 immature and mature EHTs. (B) Quantification of left- and right-side pillar displacement associated with EHT contractions in day 17–20 immature and mature EHTs from 3 independent experiments (n = 6–11). (C) Quantification of the contractile force normalized by cross-sectional areas (CSAs) of day 17–20 immature and mature EHTs from 3 independent experiments (n = 6–11). (D) Representative waveforms of intracellular calcium concentration of day 20 immature and mature EHTs. (E) Quantification of calcium uptake velocity of day 18–20 immature and mature EHTs from 3 independent experiments (n = 4–5). (F) Quantification of MitoTracker fluorescence intensity in day 13–14 immature and mature EHTs after replating from 3 independent experiments (n = 5–6). Data are presented as the mean ± SD (B, C, E, and F). Statistical analyses were performed using one-way ANOVA with Tukey's multiple comparison test (B) or unpaired t-test (C, E, and F). *, ***, and **** indicate $p < 0.05$, $p < 0.001$, and $p < 0.0001$, respectively. ns indicates not significant (B).

genes in EHTs grown on PDMS- and PS film-based devices. The results showed comparable expression levels (Fig. 6B). Moreover, we confirmed that there were no differences in major ion concentrations in the medium of EHTs between PDMS- and PS film-based devices, indicating that the device material did not affect the medium composition or consumption (Fig. 6C). Additionally, both EHTs, before and after doxorubicin treatment, responded to 1.5 Hz electrical pacing, which was the measurement condition for contractile force (Fig. 6D). Although doxorubicin treatment for 3 days reduced the contractile force of EHTs on PS film-based devices, doxorubicin-treated EHTs on PDMS-based devices did not reveal any significant changes in contractile force (Fig. 6E), consistent with a previous report by Arefin *et al.*, showing that EHTs on PDMS-based devices failed to exhibit a reduction in contractile force at concentrations of 125 nM and 500 nM doxorubicin, while treatment with 1000 nM doxorubicin significantly decreased the contractile force.[5] These results indicate that PS film-based devices prevent doxorubicin absorption, thus allowing for accurate evaluation of the cardiotoxic effects of doxorubicin on the human heart.

Discussion

In vitro organ-on-chip and microphysiological systems using human iPSC-derived cells enable mimicry of *in vivo* tissue environments not only for heart tissues but also for the liver, lungs, and multiorgan systems.[35] These *in vitro* platforms provide insights into human pharmacokinetic and pharmacodynamic properties of drugs. PDMS is a widely used biomaterial due to its advantageous features, including low cost, ease of use, optical transparency, and biocompatibility.[25] For EHT devices, the low Young's modulus of PDMS is advantageous for calculating contractile functions based on beam theory. However, the absorption of small molecules by PDMS is a significant issue when assessing pharmacokinetic and pharmacodynamic profiles. Many therapeutic agents, including estrogen and heart disease medications such as bepridil, are absorbed by PDMS, resulting in low effective drug concentrations—less than one-tenth of the expected values—depending on the physicochemical properties of the drug.[36,37] These findings are based on culturing in devices like organ-on-chips, made of PDMS substrates,

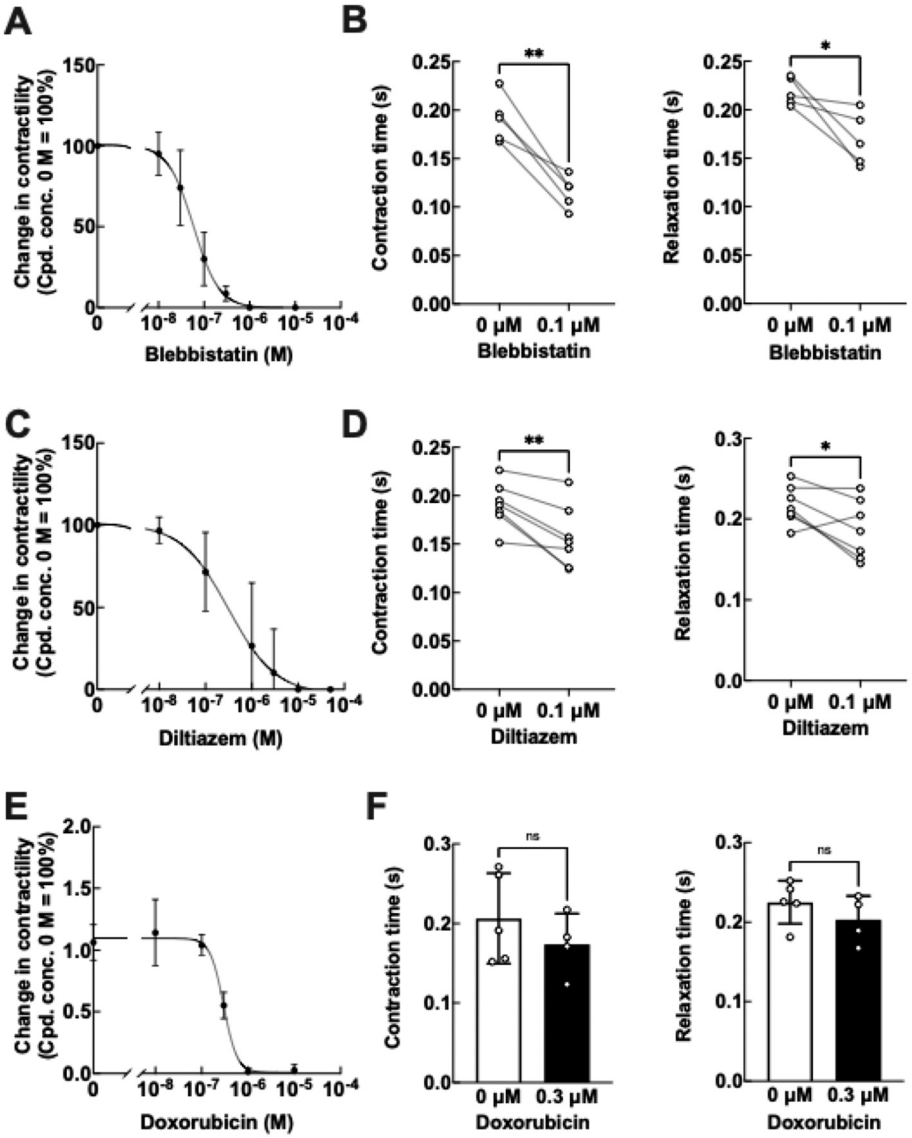

Fig. 5 Effect of acute and chronic drug exposure on contractile functions of EHTs on PS film-based devices. (A) Concentration–response curve for short-term blebbistatin treatment on the contractile force, fitted with a four-parameter model under 1.5 Hz electrical pacing from 3 independent experiments (n = 5). IC_{50} = 5.9 × 10^{-8} M. (B) Contraction and relaxation times of DMSO or 0.1 μM blebbistatin-treated EHTs under 1.5 Hz electrical pacing from 3 independent experiments (n = 5). (C) Concentration–response curve for acute diltiazem treatment on the contractile force, fitted with a four-parameter model under 1.5 Hz electrical pacing from 5 independent experiments (n = 7). IC_{50} = 3.2 × 10^{-7} M. (D) Contraction and relaxation times of DMSO or 0.1 μM diltiazem-treated EHTs under 1.5 Hz electrical pacing from 3 independent experiments (n = 7). (E) Concentration–response curve for 3 day doxorubicin treatment on the contractile force, fitted with a four-parameter model under 1.5 Hz electrical pacing from 3 independent experiments (n = 4–5). IC_{50} = 3.0 × 10^{-7} M. (F) Contraction and relaxation times of DMSO or 0.3 μM doxorubicin-treated EHTs under 1.5 Hz electrical pacing from 3 independent experiments (n = 4–5). Data are presented as the mean ± SD (A, C, E, and F). Statistical analyses were performed using paired (B and D) and unpaired t-tests (F). * and ** indicate $p < 0.05$, and $p < 0.01$, respectively. ns indicates not significant (B, D and F).

where the interface in contact with the medium is larger than in EHT devices. In the case of EHT devices, the impact of PDMS absorption on the results of *in vitro* drug testing platforms has been unclear due to a smaller contact area, thus potentially reducing the effects by absorption. Nonetheless, our study demonstrates clearly that absorption by PDMS in EHT devices affects the results, highlighting the importance of using low-absorption materials for *in vitro* drug testing platforms.

Lipid-based coatings have been used in attempts to reduce absorption by PDMS but have shown limited effects.[37] Consequently, alternative elastomers, such as poly(octamethylene maleate (anhydride) citrate) (POMaC) and tetrafluoroethylene propylene (FEPM), have been developed to mitigate absorption.[8,25] Compared to these materials, thermoplastics such as PS, which we used in this study, offer advantages, including low fabrication cost, optical clarity, and higher resolution within the design. However, the

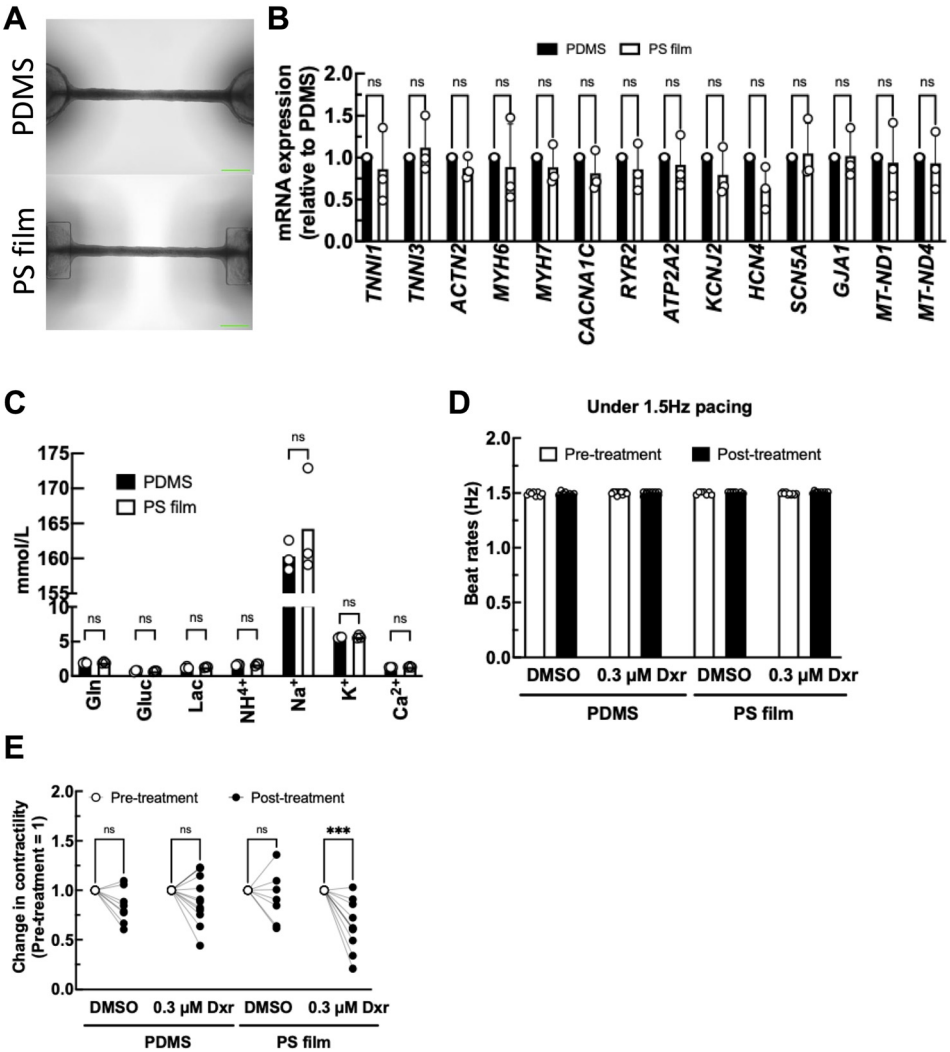

Fig. 6 Comparison of drug sensitivity between EHTs on PS film- and PDMS-based devices. (A) Representative images of day 18 EHTs with PS film- and PDMS-based devices. Scale bar: 1000 μm. (B) Quantification of selected gene expression in day 17–18 EHTs on PS film- and PDMS-based devices from 3 independent experiments (n = 3). (C) Quantification of glutamine (Gln), glucose (Gluc), lactate (Lac), NH^{4+}, Na^{+}, K^{+}, and Ca^{2+} concentrations in the culture supernatant of day 16 EHTs (D) Quantification of beating rates of EHTs on PS film- and PDMS-based devices before and after treatment with DMSO or 0.3 μM doxorubicin for 3 days under 1.5 Hz electrical pacing from 4–5 independent experiments (n = 7–12). (E) Quantification of contractile force under 1.5 Hz electrical pacing of DMSO or 0.3 μM doxorubicin-treated (3 days) EHTs on PS film- and PDMS-based devices from 4–5 independent experiments (n = 7–12). Data are presented as the mean ± SD (B–E). Statistical analyses were performed using two-way ANOVA with Šídák's multiple comparison test (B and C) or Tukey's multiple comparison test (E). *** indicates $p < 0.001$. ns indicates not significant (B, C, and E).

Young's modulus of PS (2611 MPa) is much higher than these elastomers (*e.g.*, FEPM: 0.8 MPa) (Fig. 1D), posing a major challenge for its application in EHT devices where pillars must move variably based on contractile force. To address this issue, we utilized film-shaped pillars in EHT devices to achieve a high success rate in EHT generation.

For analysis, the ability to assess contractile functions using only videos is highly versatile, as no specialized equipment is required. In contrast, manual analysis necessitates that the analyst selects the frames representing the peak and baseline from the video and measures the distance manually, thus potentially introducing bias into the analysis. Therefore, we established a unique analysis program in which the baseline and peak positions of the pillar can be automatically obtained by simply setting the pillar as an ROI, resulting in easy and accurate measurements without bias.

Conclusions

In this study, we developed an EHT device using PS, which exhibits low absorption properties. The PS film-based device and our newly developed analysis program enabled EHT generation at a high success rate and the calculation of contractile properties from pillar displacement associated with the contraction of the EHTs, respectively. Our platform

detected increases in the contractile force associated with EHT maturation and the negative inotropic effects of diltiazem and blebbistatin on EHT contractile functions. Moreover, the PS film-based EHT device detected the doxorubicin-induced impairment of contractile force even at low concentrations, which was undetectable previously in PDMS-based EHT devices. This study highlights the effects of absorption by device materials and the importance of utilizing low-absorption EHT devices to assess accurately the pharmacodynamic effects on cardiac functions. Our findings here could potentially improve the accuracy of drug evaluation to predict human efficacy and toxicity *in vitro* and contribute to a reduction in animal experiments.

Data availability

The numeric data in each graph have been included as ESI.† The source code of our contraction analysis program was deposited in GitHub (**https://github.com/Contraction-Analysis/EHT-Contraction-Analysis**). All data are available from the corresponding authors upon request.

Author contributions

Y. Fujiwara, K. Imahashi, and Y. Yoshida conceived and designed the project. Y. Fujiwara, M. Sasaki, S. Funaoka, T. Yoshikuni, Y. Naka, and K. Ida performed the experiments. M. Sasaki and Y. Fujiwara designed and wrote the analysis program. Y. Fujiwara, S. Funaoka, T. Aihara, and T. Yoshikuni designed and developed the devices. Y. Fujiwara, S. Funakoshi, and Y. Yoshida wrote the manuscript. All authors discussed the results.

Conflicts of interest

Y. Yoshida and S. Funakoshi are scientific advisors of Orizuru Therapeutics, Inc. Y. Yoshida received research funding from Takeda Pharmaceutical Co., Ltd., and Altos Labs, Inc. Y. Yoshida owns stock in iPS Portal, Inc. K. Imahashi is an employee of Takeda Pharmaceutical Co., Ltd. S. Funaoka, T. Aihara, and T. Yoshikuni are employees of Sumitomo Bakelite Co., Ltd. Y. Fujiwara, S. Funaoka, and Y. Yoshida are inventors of the patent application for the device structure (JP2023-212899). The other authors declare no competing interests.

Acknowledgements

This work was supported by the Takeda-CiRA collaboration program and by grants from Takeda Pharmaceutical Co., Ltd., Sumitomo Bakelite Co., Ltd., JSPS KAKENHI (20K16218 and 24K19055), and the Kyoto University Foundation. This work was also partially supported by grants from the Leducq Foundation (18CVD05), the Research Center Network for Realization of Regenerative Medicine, AMED (JP20bm0104001 and JP21bm0804022), the Acceleration Program of R&D and Implementation for Regenerative Medicine and Cell and Gene Therapy, AMED (JP23bm1423011, JP23bm1323001, JP24bm1123054), the Research on Regulatory Science of Pharmaceuticals and Medical Devices, AMED (JP22mk0101241, JP24mk0121280), the Program for Creating Deep Tech Startups with Global Reach, Japan Science and Technology Agency (JPMJSF2323), and the iPS Cell Research Fund. We thank Drs. Shinya Yamanaka and Yasushi Kajii for supporting this project. We thank Hiroko Sata, Rumi Fujihara, Tomomi Gibson, Mikako Marx-Mori, and Yumi Monnai for their administrative support. We also thank Kelvin Hui (CiRA) for proofreading the manuscript. In preparing this work, the authors used ChatGPT to proofread the manuscript. The authors reviewed and edited the content as needed and will take full responsibility for the content of this publication.

Notes and references

1 R. K. Harrison, *Nat. Rev. Drug Discovery*, 2016, **15**, 817–818.
2 N. Milani-Nejad and P. M. Janssen, *Pharmacol. Ther.*, 2014, **141**, 235–249.
3 Y. Fujiwara, K. Miki, K. Deguchi, Y. Naka, M. Sasaki, A. Sakoda, M. Narita, S. Imaichi, T. Sugo, S. Funakoshi, T. Nishimoto, K. Imahashi and Y. Yoshida, *Stem Cell Rep.*, 2023, **18**, 2108–2122.
4 I. Fernandes, S. Funakoshi, H. Hamidzada, S. Epelman and G. Keller, *Nat. Commun.*, 2023, **14**, 8183.
5 A. Arefin, M. Mendoza, K. Dame, M. I. Garcia, D. G. Strauss and A. J. S. Ribeiro, *Front. Pharmacol.*, 2023, **14**, 1212092.
6 Y. Qu, N. Feric, I. Pallotta, R. Singh, R. Sobbi and H. M. Vargas, *J. Pharmacol. Toxicol. Methods*, 2020, **105**, 106886.
7 R. J. Mills, B. L. Parker, G. A. Quaife-Ryan, H. K. Voges, E. J. Needham, A. Bornot, M. Ding, H. Andersson, M. Polla, D. A. Elliott, L. Drowley, M. Clausen, A. T. Plowright, I. P. Barrett, Q. D. Wang, D. E. James, E. R. Porrello and J. E. Hudson, *Cell Stem Cell*, 2019, **24**, 895–907, e896.
8 Y. Zhao, N. Rafatian, N. T. Feric, B. J. Cox, R. Aschar-Sobbi, E. Y. Wang, P. Aggarwal, B. Zhang, G. Conant, K. Ronaldson-Bouchard, A. Pahnke, S. Protze, J. H. Lee, L. Davenport Huyer, D. Jekic, A. Wickeler, H. E. Naguib, G. M. Keller, G. Vunjak-Novakovic, U. Broeckel, P. H. Backx and M. Radisic, *Cell*, 2019, **176**, 913–927, e918.
9 M. Tiburcy, J. E. Hudson, P. Balfanz, S. Schlick, T. Meyer, M. L. Chang Liao, E. Levent, F. Raad, S. Zeidler, E. Wingender, J. Riegler, M. Wang, J. D. Gold, I. Kehat, E. Wettwer, U. Ravens, P. Dierickx, L. W. van Laake, M. J. Goumans, S. Khadjeh, K. Toischer, G. Hasenfuss, L. A. Couture, A. Unger, W. A. Linke, T. Araki, B. Neel, G. Keller, L. Gepstein, J. C. Wu and W. H. Zimmermann, *Circulation*, 2017, **135**, 1832–1847.
10 A. Hansen, A. Eder, M. Bonstrup, M. Flato, M. Mewe, S. Schaaf, B. Aksehirlioglu, A. P. Schwoerer, J. Uebeler and T. Eschenhagen, *Circ. Res.*, 2010, **107**, 35–44.
11 T. Takada, D. Sasaki, K. Matsuura, K. Miura, S. Sakamoto, H. Goto, T. Ohya, T. Iida, J. Homma, T. Shimizu and N. Hagiwara, *Biomaterials*, 2022, **281**, 121351.

12 D. Zhang, I. Y. Shadrin, J. Lam, H. Q. Xian, H. R. Snodgrass and N. Bursac, *Biomaterials*, 2013, **34**, 5813–5820.
13 I. Y. Shadrin, B. W. Allen, Y. Qian, C. P. Jackman, A. L. Carlson, M. E. Juhas and N. Bursac, *Nat. Commun.*, 2017, **8**, 1825.
14 J. Li, L. Zhang, L. Yu, I. Minami, S. Miyagawa, M. Horning, J. Dong, J. Qiao, X. Qu, Y. Hua, N. Fujimoto, Y. Shiba, Y. Zhao, F. Tang, Y. Chen, Y. Sawa, C. Tang and L. Liu, *Commun. Biol.*, 2020, **3**, 122.
15 R. A. Li, W. Keung, T. J. Cashman, P. C. Backeris, B. V. Johnson, E. S. Bardot, A. O. T. Wong, P. K. W. Chan, C. W. Y. Chan and K. D. Costa, *Biomaterials*, 2018, **163**, 116–127.
16 K. Ronaldson-Bouchard, S. P. Ma, K. Yeager, T. Chen, L. Song, D. Sirabella, K. Morikawa, D. Teles, M. Yazawa and G. Vunjak-Novakovic, *Nature*, 2018, **556**, 239–243.
17 H. Vandenburgh, J. Shansky, F. Benesch-Lee, V. Barbata, J. Reid, L. Thorrez, R. Valentini and G. Crawford, *Muscle Nerve*, 2008, **37**, 438–447.
18 A. Rhoden, T. Schulze, N. Pietsch, T. Christ, A. Hansen and T. Eschenhagen, *Am. J. Physiol.*, 2022, **322**, H373–H385.
19 W. Keung, P. K. W. Chan, P. C. Backeris, E. K. Lee, N. Wong, A. O. T. Wong, G. K. Y. Wong, C. W. Y. Chan, B. Fermini, K. D. Costa and R. A. Li, *Clin. Pharmacol. Ther.*, 2019, **106**, 402–414.
20 N. T. Feric, I. Pallotta, R. Singh, D. R. Bogdanowicz, M. M. Gustilo, K. W. Chaudhary, R. N. Willette, T. P. Chendrimada, X. Xu, M. P. Graziano and R. Aschar-Sobbi, *Toxicol. Sci.*, 2019, **172**, 89–97.
21 T. A. Moore, P. Brodersen and E. W. K. Young, *Anal. Chem.*, 2017, **89**, 11391–11398.
22 S. Deguchi, M. Tsuda, K. Kosugi, A. Sakamoto, N. Mimura, R. Negoro, E. Sano, T. Nobe, K. Maeda, H. Kusuhara, H. Mizuguchi, F. Yamashita, Y. S. Torisawa and K. Takayama, *ACS Biomater. Sci. Eng.*, 2021, **7**, 3648–3657.
23 M. A. Iyer and D. Eddington, *Lab Chip*, 2019, **19**, 574–579.
24 J. Schindelin, I. Arganda-Carreras, E. Frise, V. Kaynig, M. Longair, T. Pietzsch, S. Preibisch, C. Rueden, S. Saalfeld, B. Schmid, J. Y. Tinevez, D. J. White, V. Hartenstein, K. Eliceiri, P. Tomancak and A. Cardona, *Nat. Methods*, 2012, **9**, 676–682.
25 S. B. Campbell, Q. Wu, J. Yazbeck, C. Liu, S. Okhovatian and M. Radisic, *ACS Biomater. Sci. Eng.*, 2021, **7**, 2880–2899.
26 K. Domansky, J. D. Sliz, N. Wen, C. Hinojosa, G. Thompson, J. P. Fraser, T. Hamkins-Indik, G. A. Hamilton, D. Levner and D. E. Ingber, *Microfluid. Nanofluid.*, 2017, **21**, 107.
27 E. Karbassi, A. Fenix, S. Marchiano, N. Muraoka, K. Nakamura, X. Yang and C. E. Murry, *Nat. Rev. Cardiol.*, 2020, **17**, 341–359.
28 M. J. Birket, M. C. Ribeiro, G. Kosmidis, D. Ward, A. R. Leitoguinho, V. van de Pol, C. Dambrot, H. D. Devalla, R. P. Davis, P. G. Mastroberardino, D. E. Atsma, R. Passier and C. L. Mummery, *Cell Rep.*, 2015, **13**, 733–745.
29 R. Truitt, A. Mu, E. A. Corbin, A. Vite, J. Brandimarto, B. Ky and K. B. Margulies, *JACC: Basic Transl. Sci.*, 2018, **3**, 265–276.
30 M. Mao, X. Qu, Y. Zhang, B. Gu, C. Li, R. Liu, X. Li, H. Zhu, J. He and D. Li, *Nat. Commun.*, 2023, **14**, 2077.
31 S. Funakoshi, I. Fernandes, O. Mastikhina, D. Wilkinson, T. Tran, W. Dhahri, A. Mazine, D. Yang, B. Burnett, J. Lee, S. Protze, G. D. Bader, S. S. Nunes, M. Laflamme and G. Keller, *Nat. Commun.*, 2021, **12**, 3155.
32 G. P. Farman, K. Tachampa, R. Mateja, O. Cazorla, A. Lacampagne and P. P. de Tombe, *Pflugers Arch*, 2008, **455**, 995–1005.
33 M. Honda, J. Kiyokawa, M. Tabo and T. Inoue, *J. Pharmacol. Sci.*, 2011, **117**, 149–159.
34 A. N. Linders, I. B. Dias, T. Lopez Fernandez, C. G. Tocchetti, N. Bomer and P. Van der Meer, *npj Aging*, 2024, **10**, 9.
35 D. Huh, G. A. Hamilton and D. E. Ingber, *Trends Cell Biol.*, 2011, **21**, 745–754.
36 K. J. Regehr, M. Domenech, J. T. Koepsel, K. C. Carver, S. J. Ellison-Zelski, W. L. Murphy, L. A. Schuler, E. T. Alarid and D. J. Beebe, *Lab Chip*, 2009, **9**, 2132–2139.
37 B. J. van Meer, H. de Vries, K. S. A. Firth, J. van Weerd, L. G. J. Tertoolen, H. B. J. Karperien, P. Jonkheijm, C. Denning, A. P. IJzerman and C. L. Mummery, *Biochem. Biophys. Res. Commun.*, 2017, **482**, 323–328.